Journal of Molecular and Cellular Cardiology 185 (2023) 65–76

Contents lists available at ScienceDirect

Journal of Molecular and Cellular Cardiology

journal homepage: www.elsevier.com/locate/yjmcc

Characterization of heterozygous and homozygous mouse models with the most common hypertrophic cardiomyopathy mutation *MYBPC3*$_{c.2373InsG}$ in the Netherlands

Sarah Hilderink [a,b], Maike Schuldt [a,b], Max Goebel [a,b], Valentijn J. Jansen [a,b], Emmy Manders [a], Stan Moorman [a,b], Larissa M. Dorsch [a,b], Frank G. van Steenbeek [c,d,e], Jolanda van der Velden [a,b], Diederik W.D. Kuster [a,b,*]

[a] Amsterdam UMC Location Vrije Universiteit Amsterdam, Physiology, De Boelelaan 1118, Amsterdam, the Netherlands
[b] Amsterdam Cardiovascular Sciences, Heart Failure & Arrhythmias, Amsterdam, the Netherlands
[c] Department of Clinical Sciences, Faculty of Veterinary Medicine, Utrecht University, 3584 CL Utrecht, the Netherlands
[d] Department of Cardiology, Division Heart & Lungs, University Medical Center Utrecht, Utrecht University, 3508 GA Utrecht, the Netherlands
[e] Regenerative Medicine Center Utrecht, University Medical Center Utrecht, Utrecht University, 3584 CT Utrecht, the Netherlands

ARTICLE INFO

Keywords:
Hypertrophic cardiomyopathy
Cardiac myosin binding protein c
Microtubule remodeling
Diastolic dysfunction
Mouse model

ABSTRACT

Hypertrophic cardiomyopathy (HCM) is frequently caused by mutations in the cardiac myosin binding protein-C (cMyBP-C) encoding gene *MYBPC3*. In the Netherlands, approximately 25% of patients carry the *MYBPC3-c.2373InsG* founder mutation. Most patients are heterozygous (*MYBPC3*$^{+/InsG}$) and have highly variable phenotypic expression, whereas homozygous (*MYBPC3*$^{InsG/InsG}$) patients have severe HCM at a young age. To improve understanding of disease progression and genotype-phenotype relationship based on the hallmarks of human HCM, we characterized mice with CRISPR/Cas9-induced heterozygous and homozygous mutations. At 18–28 weeks of age, we assessed the cardiac phenotype of *Mybpc3*$^{+/InsG}$ and *Mybpc3*$^{InsG/InsG}$ mice with echocardiography, and performed histological analyses. Cytoskeletal proteins and cardiomyocyte contractility of 3–4 week old and 18–28 week old *Mybpc3*$_{c.2373InsG}$ mice were compared to wild-type (WT) mice. Expectedly, knock-in of *Mybpc3*$_{c.2373InsG}$ resulted in the absence of cMyBP-C and our 18–28 week old homozygous *Mybpc3*$_{c.2373InsG}$ model developed cardiac hypertrophy and severe left ventricular systolic and diastolic dysfunction, whereas HCM was not evident in *Mybpc3*$^{+/InsG}$ mice. *Mybpc3*$^{InsG/InsG}$ cardiomyocytes also presented with slowed contraction-relaxation kinetics, to a greater extent in 18–28 week old mice, partially due to increased levels of detyrosinated tubulin and desmin, and reduced cardiac troponin I (cTnI) phosphorylation. Impaired cardiomyocyte contraction-relaxation kinetics were successfully normalized in 18–28 week old *Mybpc3*$^{InsG/InsG}$ cardiomyocytes by combining detyrosination inhibitor parthenolide and β-adrenergic receptor agonist isoproterenol. Both the 3–4 week old and 18–28 week old *Mybpc3*$^{InsG/InsG}$ models recapitulate HCM, with a severe phenotype present in the 18–28 week old model.

1. Introduction

Hypertrophic cardiomyopathy (HCM) is the most common inherited cardiac disease with a worldwide prevalence of 1:200–1:500 [1]. HCM is clinically defined by increased left ventricle (LV) wall thickness and is typically accompanied by impaired relaxation and increased risk of arrhythmias [2]. HCM is frequently caused by mutations in sarcomere protein encoding genes, with the majority of HCM cases attributed to a truncating mutation in the gene *MYBPC3*, encoding cardiac myosin binding protein C (cMyBP-C) [1,3]. The majority of *MYBPC3* mutations have been identified in single families, although a few mutations have spread and become prevalent within populations, known as founder mutations. The most prevalent *MYBPC3* founder mutation in the Netherlands is c.2373InsG, accounting for approximately 25% of HCM cases [4]. Insertion of guanine (p.Trp792fs) creates a frameshift mutation, with an alternative splice site generating a premature stop codon,

* Corresponding author at: Physiology, Amsterdam UMC, De Boelelaan 1118, 1081 HZ Amsterdam, the Netherlands.
E-mail address: d.kuster@amsterdamumc.nl (D.W.D. Kuster).

https://doi.org/10.1016/j.yjmcc.2023.10.008
Received 25 January 2023; Received in revised form 25 September 2023; Accepted 11 October 2023
Available online 14 October 2023

resulting in truncated mRNA [5].

Importantly, *MYBPC3* mutations are frameshift or missense mutations resulting in haploinsufficiency of full-length cMyBP-C [5,6]. These studies in human cardiac myectomy tissue did detect mutant mRNA in patients with a *MYBPC3* mutation, but not truncated cMyBP-C protein. In addition to cMyBP-C haploinsufficiency, cardiac tissue of HCM patients with *MYBPC3* mutations revealed reduced phosphorylation of cMyBP-C [7]. Crucially, dephosphorylated cMyBP-C interacts with myosin heavy chain S2, slowing cross-bridge kinetics [8,9]. Phosphorylation of cMyBP-C upon beta-adrenergic receptor stimulation reduces its interaction with myosin heavy chain, accelerating cross-bridge kinetics, contributing to positive lusitropic effect of adrenaline [10,11]. Phosphorylation of another contraction-associated protein, cardiac troponin I (cTnI), is also reduced in cardiac tissue of *MYBPC3* mutation carriers [5,12]. cTnI is also phosphorylated upon β-adrenergic receptor stimulation and contributes to the positive lusitropic effect of adrenaline by lowering myofilament Ca^{2+} sensitivity and accelerating cross-bridge kinetics [13,14]. Thus, reduced phosphorylation of cMyBP-C and cTnI is associated with impaired cardiac relaxation [10,11,13,14]. Diastolic dysfunction is indeed one of the first clinical signs of HCM, as impaired myocardial relaxation has been observed in the absence of cardiac hypertrophy in preclinical *MYBPC3* mutation carriers [15,16]. In addition to impaired relaxation, the HCM myocardium is characterized by myofibril disarray, hypertrophied cardiomyocytes and fibrosis [15,17].

The vast majority of HCM patients are heterozygous mutation carriers with diverse age of disease onset and heterogeneous phenotypic expression, ranging from asymptomatic to severe cardiac disease [17,18]. In contrast, a compound heterozygous or homozygous *MYBPC3* mutation results in infant death due to severe, early manifestation of HCM [18,19]. The heterogeneity of the disease hampers our understanding of the exact pathomechanisms and disease triggers associated with the initiation and progression of HCM in heterozygous patients, urging the need for an animal model that recapitulates human disease.

Gene editing with clustered regularly interspaced short palindromic repeats (CRISPR) and CRISPR-associated protein 9 (Cas9) in a mouse model allows us to closely mimic the heterozygous and homozygous genotype as present in patients [20]. Using CRISPR/Cas9 technology, we generated mice carrying the heterozygous (*Mybpc3*$^{+/InsG}$) and homozygous (*Mybpc3*$^{InsG/InsG}$) Dutch c.2373InsG founder mutation. We show that a severe cardiac phenotype in *Mybpc3*$^{InsG/InsG}$ mice is characterized by cardiac and cellular hypertrophy, and severe contractile dysfunction, while no cardiac phenotype is evident in *Mybpc3*$^{+/InsG}$ mice compared to wild-type (WT) mice at 18–28 weeks of age. In 3–4 week old *Mybpc3*$^{InsG/InsG}$ mice, contractile dysfunction is present as well. Our model recapitulates human HCM and indicates that akin to heterozygous human mutation carriers, additional disease triggers are warranted to expose a disease phenotype in heterozygous *Mybpc3* mice.

2. Methods

2.1. *Mybpc3*$_{c.2373InsG}$ mouse model

The knock-in model was generated in C75BL6/J mice, where the homozygous *MYBPC3*$_{c.2373InsG}$ (*Mybpc3*$^{InsG/InsG}$) mouse model was engineered by CRISPR/Cas9 mediated insertion of a guanine in exon 24, position 2385, on both alleles [21]. *Mybpc3*$^{+/InsG}$ mice were obtained by breeding of WT littermates with *Mybpc3*$^{InsG/InsG}$ mice.

Animals were housed according to the Guide for the Animal Care and Use Committee of the VU University Medical Center and with approval of the Animal Care Committee of the VU University Medical Center (AVD114002016700). Adult mice were phenotyped and sacrificed between 18 and 28 weeks of age. Young mice were 3–4 weeks of age.

2.2. Echocardiography

WT (4 females, 5 males), *Mybpc3*$^{+/InsG}$ (3 females, 4 males), and *Mybpc3*$^{InsG/InsG}$ (5 females, 4 males) mice (18–28 weeks old) were anesthetized with 4% (*v*/v) isoflurane and maintained under anesthesia with 2% isoflurane and mechanical ventilation (0.25 l/min O_2, 0.45 l/min air). Functional 2D echocardiography (Vevo 2100, Visualsonics, Netherlands) was recorded. From the parasternal LV-short axis (M-mode) recordings, the following parameters were determined: LV anterior and posterior wall thickness at diastole ($LVAW_d$, $LVPW_d$), LV internal diameter at diastole ($LVID_d$), and fractional shortening. From LV-long axis IVS wall thickness at diastole (IVS_d) was obtained. Pulse wave and tissue Doppler echocardiography (4 chamber view) were employed to determine isovolumetric relaxation time (IVRT) and LV filling pressure (E/e') based on the ratio of early (E) LV ventricular filling velocity to early (e') mitral annulus motion. After echocardiography, mice were killed and LV and right ventricle were weighed to determine total ventricle weight/body weight (VW/BW). For 3–4 week old mice, HW/BW of WT ($n = 2$) and *Mybpc3*$^{InsG/InsG}$ mice ($n = 3$), was determined.

2.3. Western blot

LV and apex homogenates were made as previously described [21] of 18–28 week old WT ($n = 6$), *Mybpc3*$^{+/InsG}$ ($n = 11$), and *Mybpc3*$^{InsG/InsG}$ mice (n = 6). For 3–4 week old mice, WT (n = 3) and *Mybpc3*$^{InsG/InsG}$ (n = 3) apex homogenates were made. 7 μg of protein was loaded on 4–15% precast Criterion™ gradient gels (Bio-Rad Laboratories Inc.). Proteins were separated by electrophoresis in sodium dodecyl sulfate (SDS) running buffer run at until the dye front reached the bottom of the gel. Wet tank membrane transfer to PVDF membranes ran at 0.3 A for 120 min. Membranes were blocked in 3% (*w*/*v*) bovine serum albumin (BSA) in tris-buffered saline with 0.1% (*v*/v) tween (TBS-T). Primary antibodies were incubated in 3% BSA-TBS-T overnight at 4 °C, and were as follows: Glyceraldehyde-3-Phosphate Dehydrogenase (GAPDH) 1:1000 (2118S, Cell Signaling), α-actinin 1:2500 (a7811, Sigma-Aldrich), cMyBP-C 1:3000 (sc-67,354, Santa Cruz Biotechnology), tyrosinated tubulin 1:2500 (T9028, Sigma-Aldrich), detyrosinated tubulin 1:1000 (ab48389, Abcam), desmin 1:2000 (5332S, Cell Signaling), α-tubulin 1:5000 (T9026, Sigma-Aldrich) and acetylated-α-tubulin 1:10,000 (T7451, Sigma-Aldrich), cMyBP-C pS273 1:2000, pS282 1:4000, and pS302 1:8000 (gifted from Sadayappan lab). After washing the membranes in TBS-T, secondary antibodies (goat anti-rabbit immunoglobulin G-horseradish peroxidase (IgG-HRP, 1:5000, P0448, Dako) and goat anti-mouse IgG-HRP (1:2000, P0447, Dako)) were incubated in 3% BSA-TBS-T for 1 h at room temperature. Membranes were imaged on the Amersham Imager 600 (GE Healthcare Bio-Sciences AB) or Odyssey XF (LI-COR Biosciences, USA). Protein levels relative to α-actinin or total protein stain (TPS) were determined in ImageQuant (Cytiva, USA) or Image Studio Lite (LI-COR Biosciences, USA), respectively.

2.4. Cardiac troponin I phos-tag

To analyze the phosphorylation status of cTnI, 2.5 μg protein of 18–28 week old WT ($n = 4$), *Mybpc3*$^{+/InsG}$ ($n = 5$), and *Mybpc3*$^{InsG/InsG}$ (n = 5) LV homogenates was loaded on 12% acrylamide gels containing 10 mmol/l $MnCl_2$ and 5 mmol/l Phos-Tag™ Acrylamide biotinylated probe (FUJIFILM, Wako Chemicals). Electrophoresis ran at 20–50 mA until the dye front reached the bottom of the gel. The gel was washed in ethylenediaminetetraacetic acid (EDTA)-containing transfer solution, followed by membrane transfer and blocking as performed for other western blots. Membranes were incubated overnight at 4 °C with anti-cTnI (1:1000, ab10231, Abcam). After washing the membranes in TBS-T, they were incubated with goat anti-mouse IgG-HRP (1:2000, P0447, Dako) secondary antibody for 1 h at room temperature. Membranes were imaged on the Amersham Imager 600 (GE Healthcare Bio-Sciences AB, Sweden). cTnI phosphorylation levels were determined in ImageQuant (Cytiva, USA).

2.5. Histological analyses

Paraffin-embedded coupes of 18–28 week old WT, *Mybpc3*$^{+/InsG}$, and *Mybpc3*$^{InsG/InsG}$ mouse hearts ($n = 4$, 5 μm) were deparaffinized in xylene followed by a hydration series of 100, 96, 70, and 50% ethanol, and dH_2O. The tissue was then incubated in 0.1% Picrosirius Red (Sigma-Aldrich) for 1 h followed by double washing with 0.01 mol/l HCl and dehydration in ethanol (70, 96, 100%). Excess staining was cleared by washing with xylene. Tissues were imaged on a Motic BA210 (Motic, Spain). Per heart, 10 images were analyzed with ImageJ (National Institutes of Health, USA) to determine the mean ratio of fibrosis to sarcomere size.

Similarly, the coupes of the paraffin-embedded hearts ($n = 4$, 5 μm) were also deparaffinized and hydrated to determine the size of cardiomyocytes. The tissue was stained with hematoxylin and eosin (Thermo Fisher) (H&E), followed by a dehydration series of 70, 96, and 2 × 100% ethanol, and 2× xylene. Tissues were imaged on a Motic BA210 (Motic, Spain). Per heart, five images were analyzed to quantify mean cross-sectional area (CSA) using ImageJ (National Institutes of Health, USA).

2.6. Cardiomyocyte isolation and unloaded shortening measurements

Single cardiomyocytes were isolated from 18 to 28 week old WT ($n = 5$), *Mybpc3*$^{+/InsG}$ ($n = 4$), and *Mybpc3*$^{InsG/InsG}$ mice ($n = 8$), and from 3 to 4 week old WT ($n = 3$) and *Mybpc3*$^{InsG/InsG}$ mice (n = 3) as described previously [21]. Cardiomyocytes were plated on laminin-coated dishes (10 μg/ml, Sigma-Aldrich) in Medium 199 (Lonza), supplemented with 1% penicillin/streptomycin and 5% bovine serum. Cells were incubated for 1 h at 37 °C and 5% (*v*/v) CO_2. Non-attached cells were washed off and attached cells were incubated in medium 199 (Lonza), 1% penicillin/streptomycin, 1× insulin-transferrin-sodium selenite supplement (Sigma-Aldrich), and 0.5 μmol/l cytochalasin D (Life Technologies). 18–28 week old cardiomyocytes were treated with vehicle dimethyl sulfoxide (DMSO, 0.1% v/v), or parthenolide (PTL, 10 μmol/l, Sigma-Aldrich) for 2 h at 37 °C. Cells were also measured immediately after addition of 15 nmol/l isoproterenol (ISO) (Sigma-Aldrich) to untreated cells, and to PTL-treated cells (PTL + ISO). 3–4 week old WT and *Mybpc3*$^{InsG/InsG}$ cardiomyocytes were measured under control conditions (DMSO).

Contractility was measured in modified Tyrode's solution (containing in mmol/l: 10 HEPES, 133.5 NaCl, 5 KCl, 1.2 NaH_2PO_4, 1.2 MgSO4, 11.1 glucose, 5 sodium pyruvate; pH 7.4). Measurements were performed at 37 °C with the MultiCell system (CytoCypher BV, the Netherlands) and cells were field-stimulated at 2 Hz, 25 V, and 4 ms pulse duration as described previously [21,22]. Fractional shortening, contraction time (time to peak 70%), relaxation time (time to baseline 70%), and diastolic sarcomere length (SL) were analyzed with automated video-based detection software (IonOptix, USA). Contractility measurements were included when cardiomyocytes had a minimum of 4 contraction transients during field-stimulation, and $R^2 > 0.95$ for peak and baseline fit.

2.7. Statistical analysis

Data are presented as mean ± standard error of the mean (SEM). Comparisons amongst 18–28 week old WT, *Mybpc3*$^{+/InsG}$, and *Mybpc3*$^{InsG/InsG}$ were carried out with a One-way ANOVA and Tukey's post hoc correction for multiple testing (cMyBP-C/α-actinin, VW/BW, IVSd, LVPWd, IVRT, fibrosis, cardiomyocyte CSA, detyrosinated tubulin/TPS, Tyrosinated tubulin/TPS, α-tubulin/TPS, acetylated-α-tubulin/TPS, desmin/TPS). For non-normal data, Kruskal-Wallis' nonparametric test was applied (LVAWd, and LVIDd). Independent samples *t*-test was performed when comparing two groups (E/e', and all 3–4 week old mouse data). Two-way ANOVA and Tukey's post hoc multiple testing correction were applied to compare all three groups and multiple variables (cTnI phosphorylation). Unloaded shortening data was transformed and significance was determined with hierarchical testing. A linear regression model was applied to assess the correlation between peak height and sarcomere length. Analyses were performed with GraphPad Prism 9.1.0 (GraphPad Software, USA). A *p*-value <0.05 was considered statistically significant.

3. Results

3.1. Successful generation of CRISPR/Cas9 homozygous *Mybpc3*$_{c.2373InsG}$ mice with cardiac hypertrophy

Mybpc3$^{InsG/InsG}$ mice were generated with CRISPR/Cas9 (Fig. 1A). Successful generation of the mouse model was confirmed by western blot analysis of LV lysates (WT $n = 6$, *Mybpc3*$^{+/InsG}$ $n = 11$, and *Mybpc3*$^{InsG/InsG}$ n = 6, 18–28 weeks old), which marked the complete absence of cMyBP-C in the *Mybpc3*$^{InsG/InsG}$ mice (Fig. 1B). In heterozygous *MYBPC3*$_{c.2373InsG}$ patients, no truncated cMyBP-C is detected [5]. No haploinsufficiency was detected in the *Mybpc3*$^{+/InsG}$ mice, which had cMyBP-C levels akin to WT. Cardiac hypertrophy was observed in *Mybpc3*$^{InsG/InsG}$ mice, where VW/BW nearly doubled in comparison to WT and *Mybpc3*$^{+/InsG}$ mice ($n = 9$) (Fig. 1C).

An early histopathological hallmark of HCM is cardiomyocyte enlargement [23]. Therefore, cardiomyocyte hypertrophy of our 18–28 week old *Mybpc3*$_{c.2373InsG}$ model was quantified based on cardiomyocyte cross-sectional area (CSA) by H&E staining (Fig. 1D). Cardiomyocyte CSA was increased in *Mybpc3*$^{InsG/InsG}$ hearts to 333 ± 17 μm^2 compared to 186 ± 8 μm^2 in WT and 194 ± 22 μm^2 in *Mybpc3*$^{+/InsG}$ hearts ($n = 4$) (Fig. 1E). Another pathological hallmark of HCM is myocardial fibrosis, estimated to be prevalent in 70% of HCM patients [24], although there is a large inter-patient variability in the degree of cardiac fibrosis [25,26]. We determined relative fibrosis in our mouse model by picrosirius red staining of collagen in WT, *Mybpc3*$^{+/InsG}$, and *Mybpc3*$^{InsG/InsG}$ LVs (n = 4) (Fig. 1D, F). The extent of fibrosis was similar between the three groups.

3.2. Severe cardiac dysfunction in *Mybpc3*$^{InsG/InsG}$ but not *Mybpc3*$^{+/InsG}$ mice

Mice were phenotyped with echocardiography (Fig. 2A). Increased ventricular wall thickness of *Mybpc3*$^{InsG/InsG}$ mice ($n = 7$) was evident based on a significant increase in IVS_d, $LVID_d$, and $LVAW_d$, in comparison to WT ($n = 8$) and *Mybpc3*$^{+/InsG}$ (n = 8) mice (Fig. 2B-D). $LVPW_d$ of *Mybpc3*$^{InsG/InsG}$ mice was increased compared to WT mice (Fig. 2E). Cardiac dimensions were not altered in *Mybpc3*$^{+/InsG}$ mice compared to WT.

Functionally, fractional shortening decreased by >80% in *Mybpc3*$^{InsG/InsG}$ mice, compared to WT and *Mybpc3*$^{+/InsG}$ mice (Fig. 2F). Using Pulsed-wave Doppler echocardiography, diastolic dysfunction was detected in *Mybpc3*$^{InsG/InsG}$ mice, where IVRT tripled in comparison to WT and *Mybpc3*$^{+/InsG}$ mice (Fig. 2G). LV filling pressure (E/e') could not be determined in *Mybpc3*$^{InsG/InsG}$ mice due to the merging of the e' and a' waves, but was similar in *Mybpc3*$^{+/InsG}$ and WT mice (Fig. 2H).

3.3. Cardiomyocyte contraction-relaxation kinetics are impaired in *Mybpc3*$^{InsG/InsG}$ mice

As contractility of isolated cardiomyocytes from HCM patients cannot be studied easily, our mouse model provides additional insight into cardiac function and the effect of potential therapeutic interventions. Unloaded shortening of single isolated cardiomyocytes from 18 to 28 week old WT ($N = 5$ mice, $n = 292$ cells), *Mybpc3*$^{+/InsG}$ (N/$n = 4/257$), and *Mybpc3*$^{InsG/InsG}$ (N/$n = 8/249$) mice was assessed. For baseline measurements, cardiomyocytes were exposed to 0.1% DMSO (vehicle) for 2 h. Diastolic SL of *Mybpc3*$^{InsG/InsG}$ cardiomyocytes (1.64 ± <0.01 μm) was significantly shorter than found in WT (1.81 ± <0.01 μm) and *Mybpc3*$^{+/InsG}$ (1.80 ± <0.01 μm) cardiomyocytes (Fig. 3A,

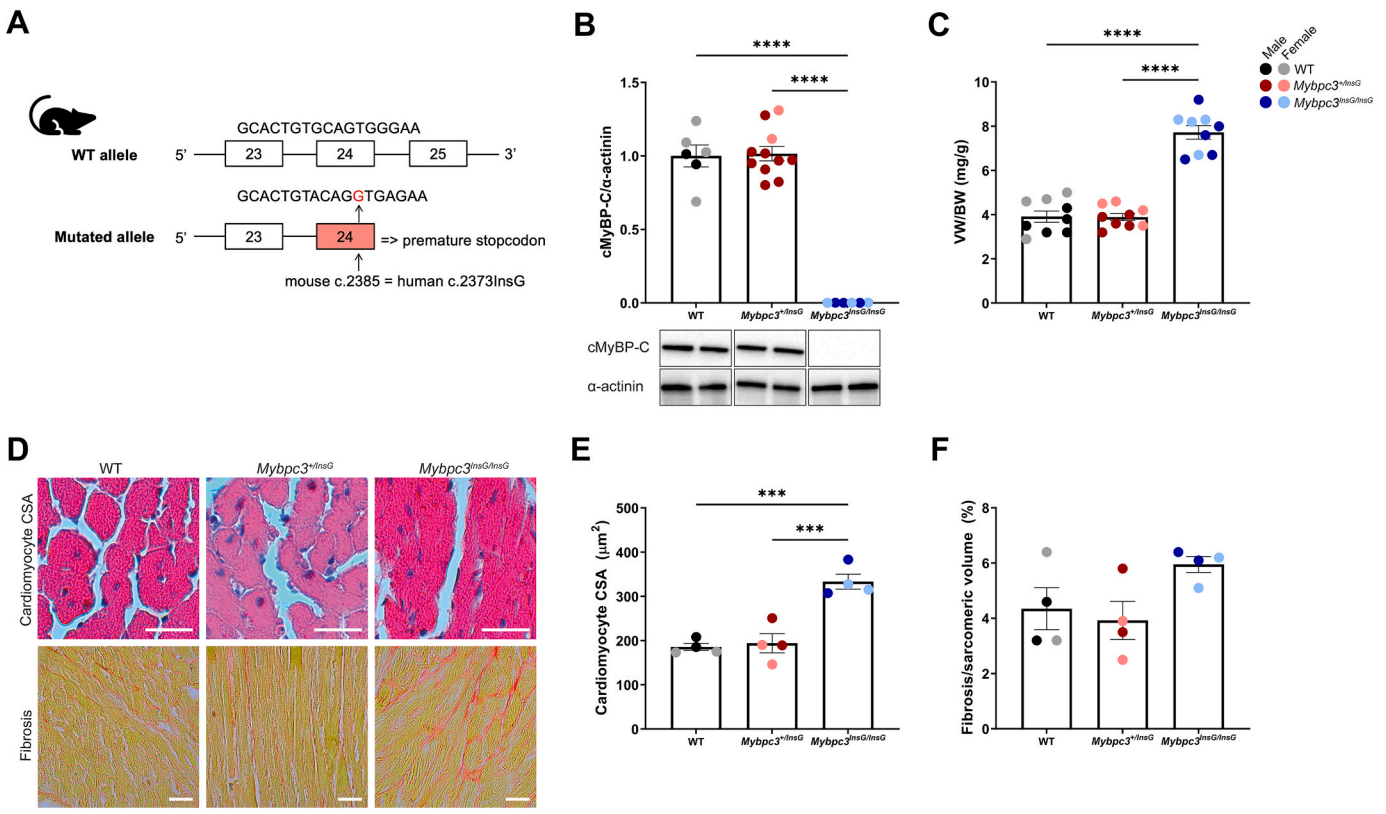

Fig. 1. Validation of CRIPSR/Cas9 engineered *Mybpc3*$^{InsG/InsG}$ knock-in mice. (A) CRISPR/Cas9 generation of homozygous *Mybpc3*$_{c.2373InsG}$ mice by introduction of a premature stop codon at exon 24 on both alleles. (B) cMyBP-C protein levels relative to α-actinin in 18–28 week old WT ($n = 6$, black), *Mybpc3*$^{+/InsG}$ ($n = 11$, red), and *Mybpc3*$^{InsG/InsG}$ (n = 6, blue) mice. (C) VW/BW (mg/g) of WT, *Mybpc3*$^{+/InsG}$, and *Mybpc3*$^{InsG/InsG}$ mice ($n = 9$). (D) Representative images of cardiomyocyte hypertrophy (H&E) and fibrosis (picrosirius red) corresponding to E,F. (E) Cardiomyocyte cross-sectional area (CSA, μm^2) and (F) cardiac fibrosis/sarcomere volume of WT, *Mybpc3*$^{+/InsG}$, and *Mybpc3*$^{InsG/InsG}$ ($n = 4$) mice. Scale bar represents 25 μm. Darker-shade symbols represent male mice. Mean ± SEM. ***$p < 0.001$, ****$p <$ 0.0001. (For interpretation of the references to colour in this figure legend, the reader is referred to the web version of this article.)

Supplementary Fig. S3B). As reported previously [21], contraction duration (time to peak 70%) and relaxation duration (time to baseline 70%) of *Mybpc3*$^{InsG/InsG}$ cardiomyocytes (0.03 ± <0.01 s and 0.053 ± <0.01 s, respectively) were prolonged compared to WT (0.023 ± <0.01 s and 0.042 ± <0.01 s, respectively) (Fig. 3C,D). Contraction-relaxation kinetics of 18–28 week old *Mybpc3*$^{+/InsG}$ cardiomyocytes were akin to WT. Fractional shortening of *Mybpc3*$^{InsG/InsG}$ (4.91 ± 0.17%) cardiomyocytes was increased compared to WT (3.57 ± 0.13%) and *Mybpc3*$^{+/InsG}$ (3.14 ± 0.12%) cardiomyocytes as well (Fig. 3B). Overall, contraction-relaxation kinetics were impaired in *Mybpc3*$^{InsG/InsG}$ mice.

3.4. Cardiomyocyte microtubule remodeling and cTnI dephosphorylation contribute to impaired relaxation and increased stiffness in *Mybpc3*$^{InsG/InsG}$ mice

A proteomics study in human myectomy samples revealed an altered signature of non-sarcomere cytoskeletal proteins, characterized by increased levels of detyrosinated and acetylated tubulin and desmin. Modified microtubule composition has been reported to alter visco-elasticity and stiffness in heart failure [27,28]. Desmin, a cytoskeletal connective protein has been reported to influence microtubule stabilization and cardiomyocyte stiffness [27]. We previously reported that expression of the non-sarcomere cytoskeletal protein desmin and detyrosinated tubulin were increased in *Mybpc3*$^{InsG/InsG}$ compared to WT mice [21].

Here, cardiac protein levels of tubulin and desmin were determined for WT ($n = 6$), *Mybpc3*$^{+/InsG}$ ($n = 11$), and *Mybpc3*$^{InsG/InsG}$ (n = 6) by western blot. Tyrosinated tubulin, α-tubulin, and acetylated α-tubulin levels were comparable amongst all groups (Fig. 4A,C,D). In line with our previous work [21], we noted increased levels of detyrosinated tubulin in *Mybpc3*$^{InsG/InsG}$ mice (2.19 ± 0.45) compared to WT (1.00 ± 0.25) and *Mybpc3*$^{+/InsG}$ (0.75 ± 0.13) (Fig. 4B). Desmin was also increased in *Mybpc3*$^{InsG/InsG}$ mice (4.44 ± 0.48) compared to WT (1.00 ± 0.13) and *Mybpc3*$^{+/InsG}$ (1.68 ± 0.13) (Fig. 4E).

Impaired cardiomyocyte relaxation in HCM is partially caused by microtubule remodeling [21,28], as well as increased myofilament Ca^{2+} sensitivity as a consequence of reduced cTnI phosphorylation [5,13,14]. Here, cTnI phosphorylation of WT, *Mybpc3*$^{+/InsG}$, and *Mybpc3*$^{InsG/InsG}$ mice was determined by Phos-Tag western blot (Fig. 4F). This revealed a significantly different cTnI phosphorylation pattern in *Mybpc3*$^{InsG/InsG}$ compared to WT hearts, with a smaller fraction of bi-phosphorylated cTnI (2P: 18.2 ± 5.1%) and more monophosphorylated cTnI (1P: 72.4 ± 3.0%) in *Mybpc3*$^{InsG/InsG}$ compared to WT (2P and 1P, 38.5 ± 5.0% and 51.4 ± 2.7%, respectively). Heterozygous mice did not have an altered cTnI phosphorylation profile, although a small increase in cMyBP-C phosphorylated serine 282 (pS282), but not 273 and 302, was seen in *Mybpc3*$^{+/InsG}$ mice, compared to WT (Supplementary Fig. S1).

3.5. Detyrosination inhibitor PTL and β-adrenergic agonist ISO rescue impaired cardiomyocyte contraction-relaxation kinetics of *Mybpc3*$^{InsG/InsG}$ mice

To investigate if modulation of detyrosinated tubulin and cTnI phosphorylation could correct hampered unloaded shortening of *Mybpc3*$^{InsG/InsG}$ cardiomyocytes, cells were treated with PTL, ISO, and a combination of PTL + ISO. Single cardiomyocytes isolated from WT (N/$n = 4/141$), *Mybpc3*$^{+/InsG}$ (N/$n = 3/128$), and *Mybpc3*$^{InsG/InsG}$ (N/$n = 7/143$) mice were incubated with detyrosination inhibitor PTL (10 μmol/l)

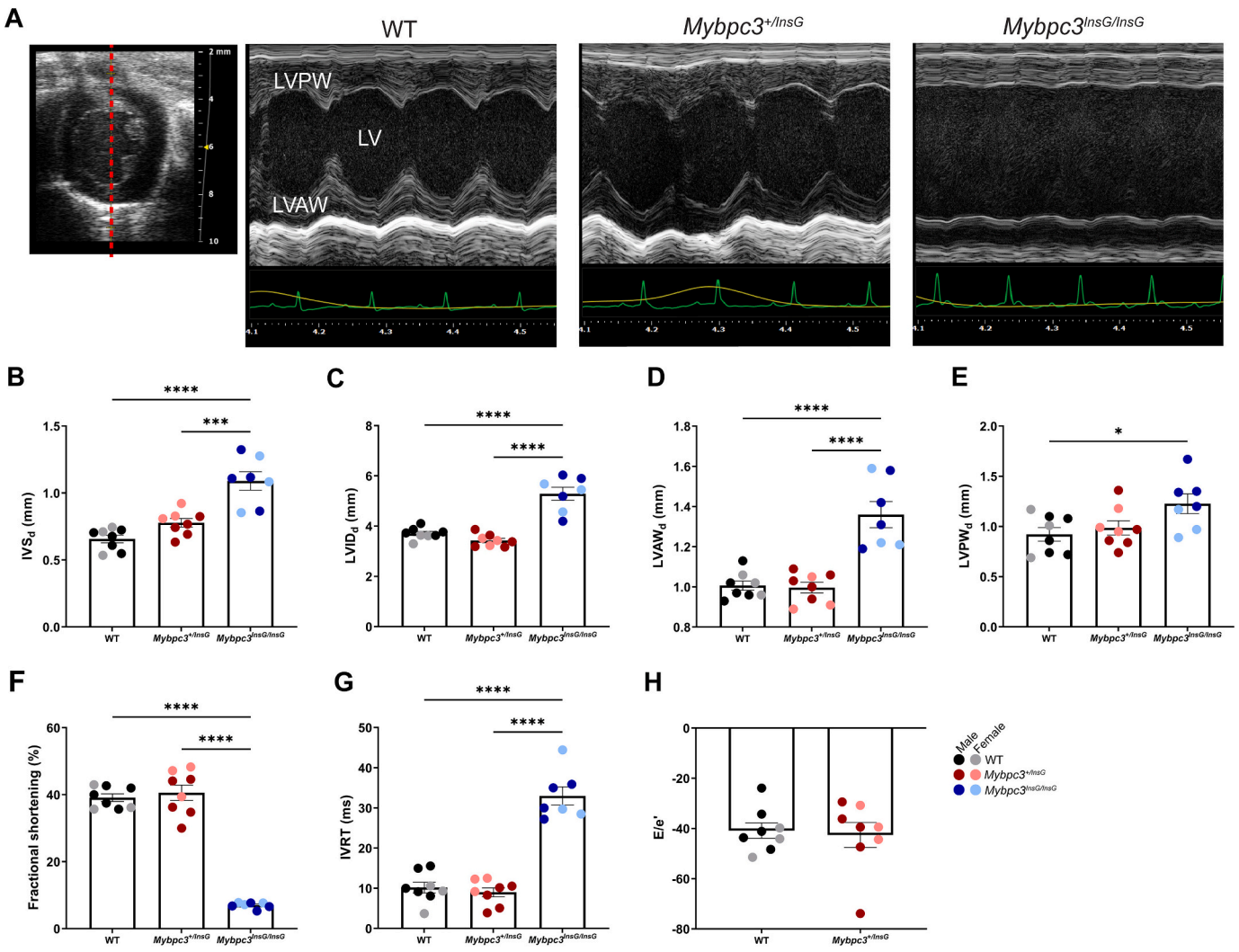

Fig. 2. Hampered cardiac function and severe hypertrophy in homozygous *Mybpc3*$_{c.2373InsG}$ mice. (A) Representative m-mode echocardiography images (dashed red line) and echo parameters for WT ($n = 8$, black), and *Mybpc3*$^{+/InsG}$ (n = 8, red), and *Mybpc3*$^{InsG/InsG}$ ($n = 7$, blue) mice. (B) Diastolic intraventricular septal thickness (IVS_d, mm). (C) Diastolic LV internal diameter ($LVID_d$, mm). (D) Diastolic LV anterior wall thickness ($LVAW_d$, mm). (E) Diastolic LV posterior wall thickness ($LVPW_d$, mm). (F) Fractional shortening (%). (G) Isovolumetric relaxation time (IVRT, ms). (H) LV filling pressure (E/e'). Darker-shade symbols represent male mice. Mean ± SEM. $^*p < 0.05$, $^{***}p < 0.001$, $^{****}p < 0.0001$. (For interpretation of the references to colour in this figure legend, the reader is referred to the web version of this article.)

for 2 h to inhibit tubulin detyrosination (Supplementary Fig. S2) after which unloaded shortening was assessed. Isolated cardiomyocytes of WT (N/n = 3/130), *Mybpc3*$^{+/InsG}$ (N/n = 4/257), and *Mybpc3*$^{InsG/InsG}$ (N/n = 5/94) were also acutely treated with 15 nmol/l ISO to stimulate β-adrenergic activity. Additionally, ISO was added to WT (N/n = 3/109), *Mybpc3*$^{+/InsG}$ (N/n = 3/131), and *Mybpc3*$^{InsG/InsG}$ (N/n = 4/45) cardiomyocytes incubated with PTL (PTL + ISO).

Addition of β -adrenergic stimulant ISO shortened relaxation time of WT, *Mybpc3*$^{+/InsG}$ and *Mybpc3*$^{InsG/InsG}$ cardiomyocytes compared to their respective vehicle baseline (Fig. 5C). This was also evident in PTL + ISO treated cells. PTL did not significantly affect relaxation time but did accelerate the rate of contractility (time to peak 70%) in all groups compared to their respective baseline, and PTL + ISO further shortened contraction time (Fig. 5D). In *Mybpc3*$^{InsG/InsG}$ cardiomyocytes, ISO treatment also shortened time to peak 70%. ISO also increased fractional shortening of WT, *Mybpc3*$^{+/InsG}$ and *Mybpc3*$^{InsG/InsG}$ cardiomyocytes (Fig. 5E).

To test if the lower diastolic sarcomere length observed in *Mybpc3*$^{InsG/InsG}$ cardiomyocytes (Fig. 5A,B, Supplementary Fig. S3B,C) would limit the increase in fractional shortening, we plotted diastolic SL and peak height, but found no correlation (Supplementary Fig. S3D). The main deficit in *Mybpc3*$^{InsG/InsG}$ cardiomyocytes was their slowed contraction and relaxation kinetics.

3.6. HCM in 3–4 week old *Mybpc3*$^{InsG/InsG}$ mice

As our adult *Mybpc3*$^{InsG/InsG}$ model displays an end-stage HCM phenotype, we sought to determine whether the mutation at an earlier stage expresses a milder phenotype resembling early-stage HCM, as found in part of the heterozygous patient population. cMyBP-C levels are also negligible in our 3–4 week old *Mybpc3*$^{InsG/InsG}$ mouse model ($n = 3$) (Fig. 6A). Cardiac hypertrophy is suggested to be present in *Mybpc3*$^{InsG/InsG}$ (n = 3) mice, as HW/BW doubled in comparison to WT ($n = 2$), although the WT sample size limits the certainty of this finding (Supplementary Fig. S4).

Protein levels of the non-sarcomere cytoskeleton which are known to be altered towards a stiffer profile in adult mice, were also assessed in our 3–4 week *Mybpc3*$^{InsG/InsG}$ model. In these mice ($n = 3$), desmin, tyrosinated tubulin, detyrosinated tubulin, and acetylated-a-tubulin, were elevated in comparison to WT ($n = 3$) (Fig. 6B-D,F). Although

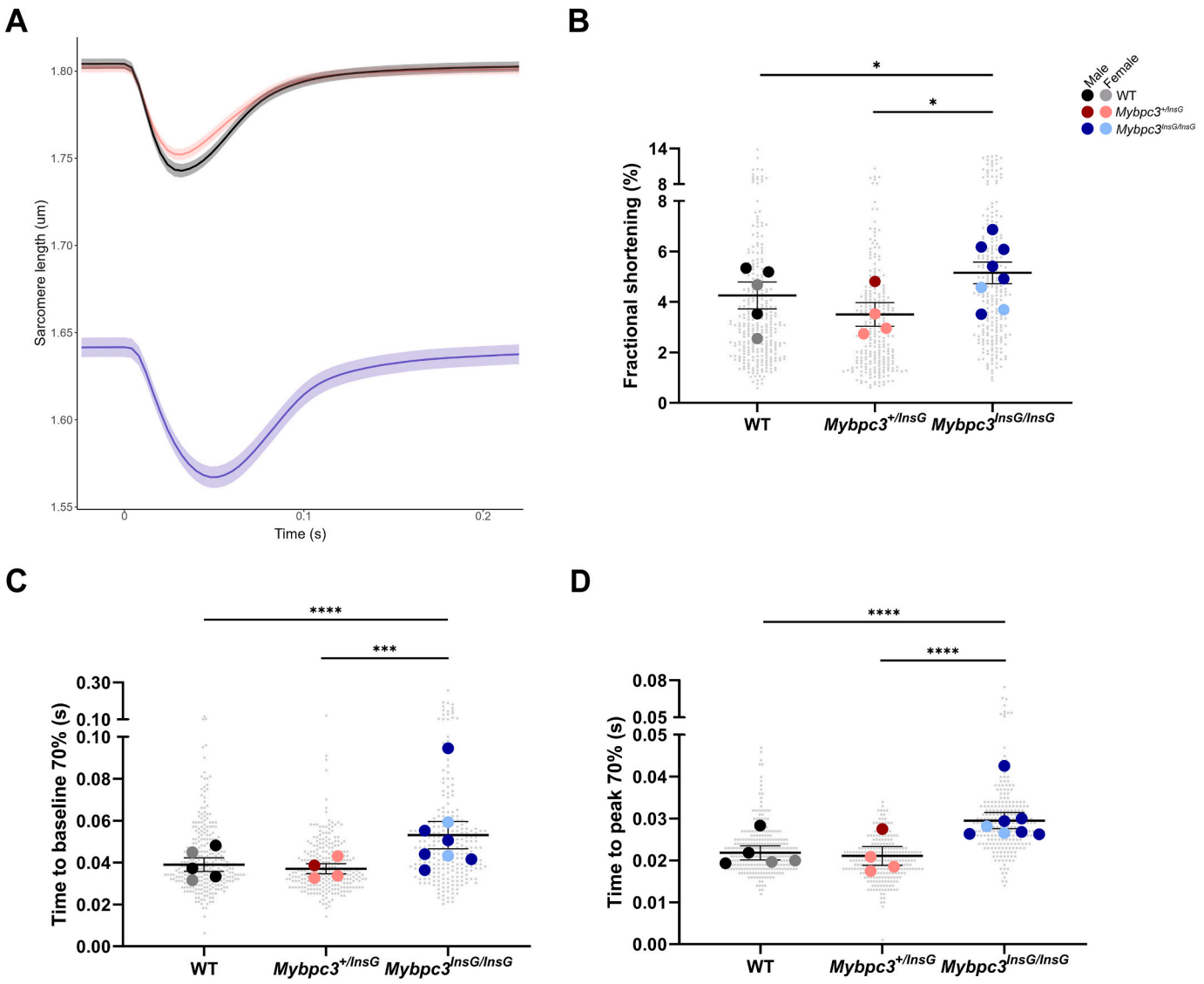

Fig. 3. Impaired cardiomyocyte function in 18–28 week old *Mybpc3*$^{InsG/InsG}$ mice. (A) Averaged contraction-relaxation traces of vehicle (0.1% DMSO) WT ($N = 5$ mice, $n = 292$ cells, black/grey), *Mybpc3*$^{+/InsG}$ (N/$n = 4/257$, red), and *Mybpc3*$^{InsG/InsG}$ (N/$n = 8/249$, blue) cardiomyocytes. (B) Fractional shortening (%), (C) Time to baseline 70% (s), (D) time to peak 70% (s). Single cardiomyocytes represented as grey dots. Darker-shade symbols represent male mice. Mean ± SEM. *$p < 0.05$, ****$p < 0.0001$. (For interpretation of the references to colour in this figure legend, the reader is referred to the web version of this article.)

not significant, α-tubulin levels of *Mybpc3*$^{InsG/InsG}$ trend towards an increase as well.

As altered composition of the cytoskeleton affects cardiac contractile kinetics, we investigated unloaded shortening of single isolated cardiomyocytes from WT (N/n = 3/294) and *Mybpc3*$^{InsG/InsG}$ (N/n = 3/208) mice. Compared to age-matched WT cardiomyocytes, contraction and relaxation duration were prolonged in *Mybpc3*$^{InsG/InsG}$ cardiomyocytes (Fig. 6H,I). A small, yet significant decrease in fractional shortening was observed in *Mybpc3*$^{InsG/InsG}$ cardiomyocytes (Fig. 6J). Akin to the 18–28 week old *Mybpc3*$^{InsG/InsG}$ model, 3–4 week old *Mybpc3*$^{InsG/InsG}$ cardiomyocytes had a shorter diastolic SL than WT cardiomyocytes (Fig. 6G, Supplementary Fig. S3A).

3.7. Differences in HCM phenotype of young and adult homozygous *Mybpc3*$_{c.2373InsG}$ mice

Our 3–4 week homozygous *Mybpc3*$_{c.2373InsG}$ model provides insight into changes associated with HCM at an earlier stage. At 3–4 weeks of age, *Mybpc3*$_{c.2373InsG}$ mice present with an altered tubulin signature. This further develops in the 18–28 week old *Mybpc3*$^{InsG/InsG}$ mice. The increase in detyrosinated tubulin is evident early on in HCM, with a 4-fold increase in 3–4 week old *Mybpc3*$^{InsG/InsG}$ mice and >2-fold increase in 18–28 week old mice compared to age-matched WT mice (Fig. 7). Tyrosinated tubulin levels were also 4-fold increased in the 3–4 week old *Mybpc3*$^{InsG/InsG}$ mice. Increase of these post-translational modifications (PTMs) requires increased total α-tubulin as well, which is present in 3–4 week old *Mybpc3*$^{InsG/InsG}$ model compared to the 18–28 week old model. Relatively, acetylated-α-tubulin increased more in the 18–28 week old *Mybpc3*$^{InsG/InsG}$ model, although it is also increased in the 3–4 week old *Mybpc3*$^{InsG/InsG}$ mice. Desmin is increased by 4-fold in 18–28 week old *Mybpc3*$^{InsG/InsG}$ mice, and to a far lesser degree in 3–4 week old *Mybpc3*$^{InsG/InsG}$ mice. Relative to their age-matched WT, rate of contractility was prolonged in 18–28 week old *Mybpc3*$^{InsG/InsG}$ mice.

4. Discussion

We describe a mouse model harboring the *Mybpc3*$_{c.2373InsG}$ mutation, where 18–28 week old homozygous mice recapitulate a phenotype representative of severely affected HCM mutation carriers, denoted by a thickened LV septum and wall, cardiomyocyte hypertrophy, and

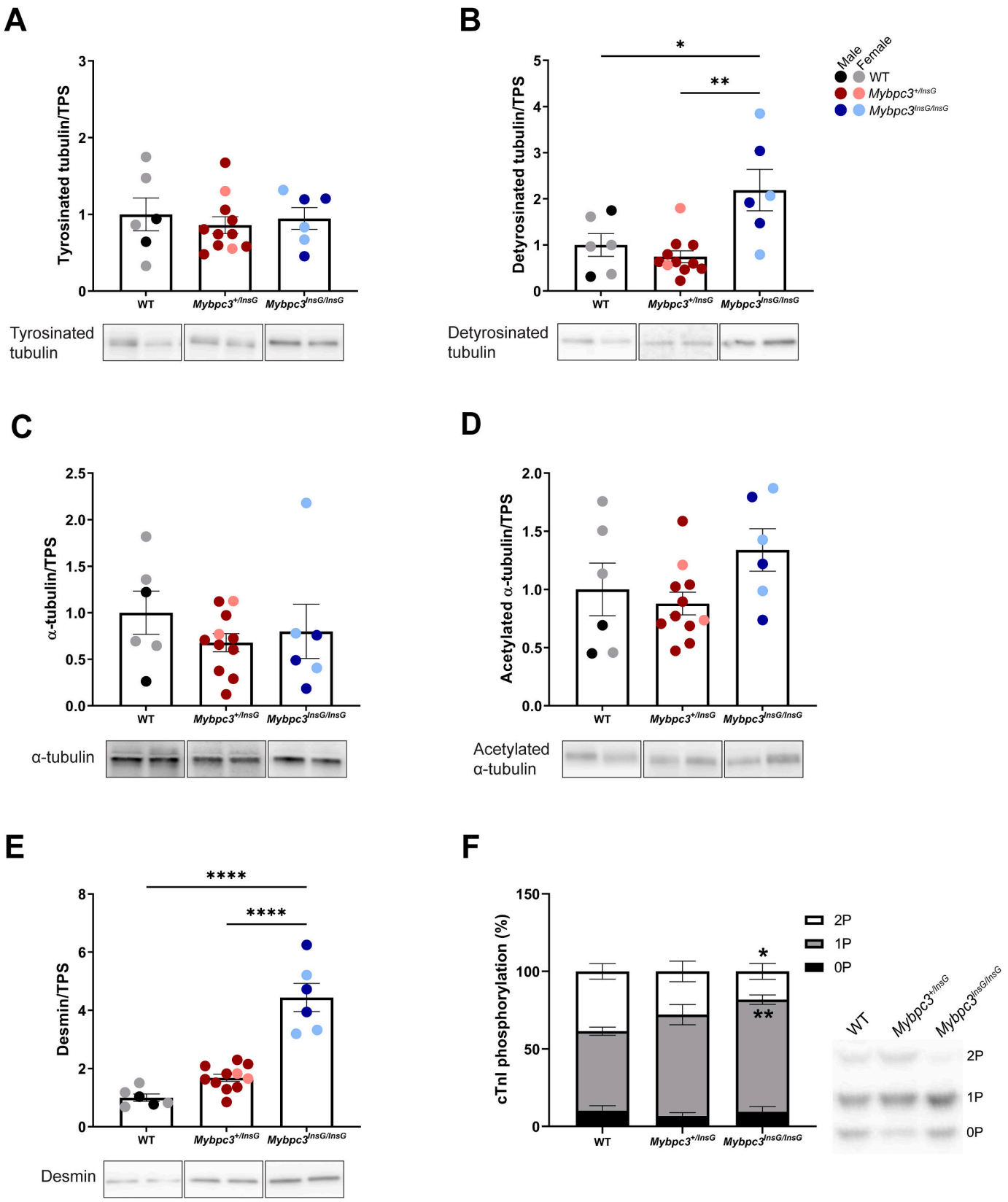

Fig. 4. Altered protein signature of cardiomyocyte contraction-relaxation determinants in *Mybpc3*$^{InsG/InsG}$ mice. Quantification of relative protein levels in 18–28 week old WT ($n = 6$, black/grey), *Mybpc3*$^{+/InsG}$ ($n = 11$, red), and *Mybpc3*$^{InsG/InsG}$ (n = 6, blue) mice and representative western blot images of (A) tyrosinated tubulin (B) detyrosinated tubulin, (C) α-tubulin, (D) acetylated α-tubulin, and (E) desmin. A-E Normalized to total protein stain (Supplementary materials). Darker-shade symbols represent male mice. Mean ± SEM. *$p < 0.05$, **$p < 0.01$, ****$p < 0.0001$. (F) Phosphorylation levels of cTnI (0P (white), 1P (grey), and 2P (black) in WT, *Mybpc3*$^{+/InsG}$, and *Mybpc3*$^{InsG/InsG}$ hearts ($n = 4, 5, 5$, respectively) and representative Phos-Tag western blot. Mean ± SEM. *p < 0.05 between WT and *Mybpc3*$^{InsG/InsG}$ 2P. **p < 0.01 between WT and *Mybpc3*$^{InsG/InsG}$ 1P. (For interpretation of the references to colour in this figure legend, the reader is referred to the web version of this article.)

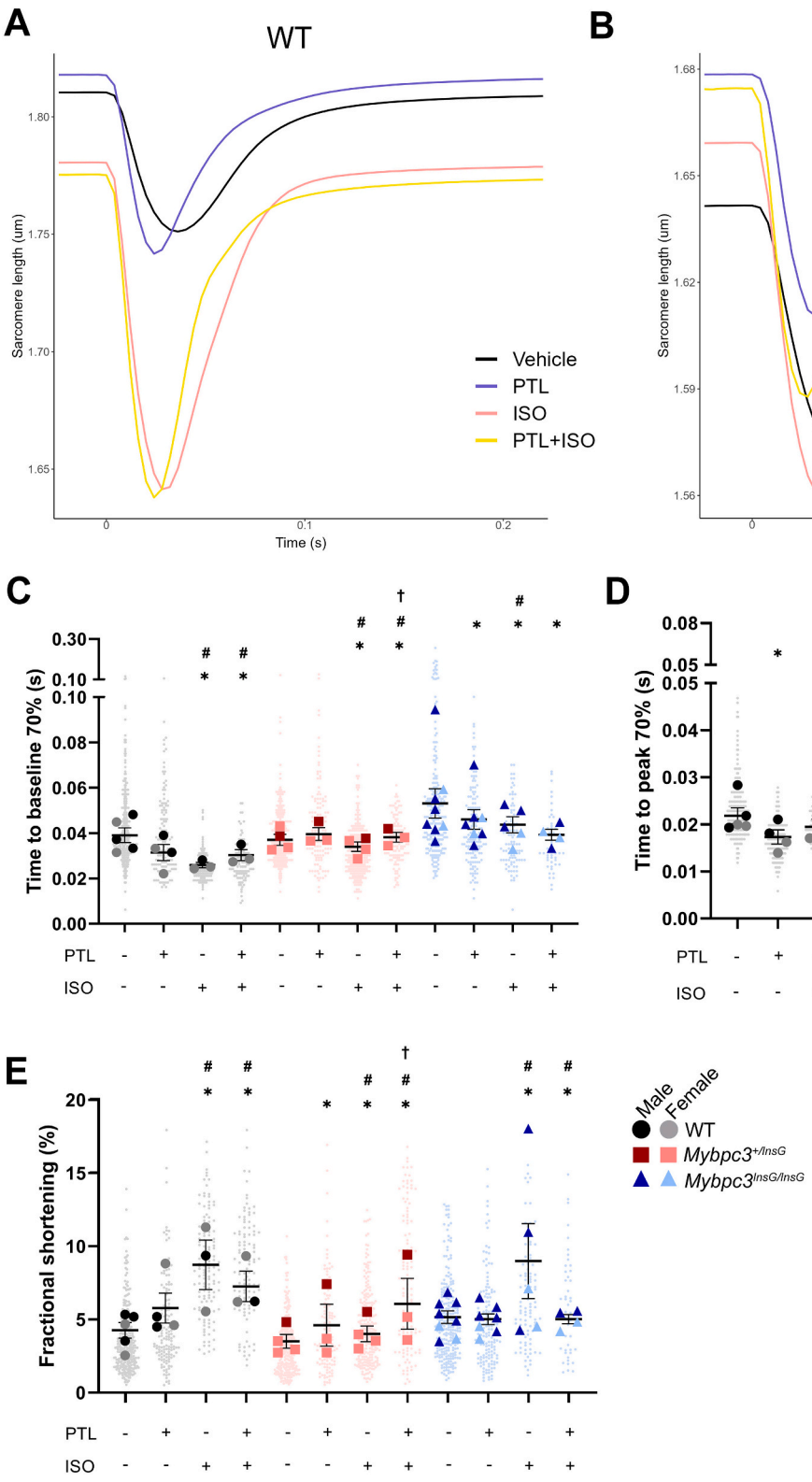

Fig. 5. Rescuing altered contraction-relaxation kinetics in *Mybpc3*$^{InsG/InsG}$ cardiomyocytes. (A-B) Mean contraction-relaxation traces of (A) WT and (B) *Mybpc3*$^{InsG/InsG}$ cardiomyocytes treated with DMSO (vehicle, black), parthenolide (PTL, 10 μmol/l, red), isoproterenol (ISO, 15 nmol/l, blue), and PTL + ISO (yellow). (C-E) Cardiomyocytes of WT (black circles), *Mybpc3*$^{+/InsG}$ (red squares), and *Mybpc3*$^{InsG/InsG}$ (blue triangles) mice were treated with DMSO (vehicle) ($N = 5$ mice, $n = 292$ cells, black), *Mybpc3*$^{+/InsG}$ (N/n = 4/257, red), and *Mybpc3*$^{InsG/InsG}$ (N/n = 8/249, blue) PTL (WT N/n = 4/141, *Mybpc3*$^{+/InsG}$ N/n = 3/128, *Mybpc3*$^{InsG/InsG}$ N/n = 7/143), ISO (WT N/n = 3/130, *Mybpc3*$^{+/InsG}$ N/n = 4/257, *Mybpc3*$^{InsG/InsG}$ N/n = 5/94), or PTL + ISO (WT N/n = 3/109, *Mybpc3*$^{+/InsG}$ N/n = 3/131, *Mybpc3*$^{InsG/InsG}$ N/n = 4/45). (C) Time to baseline 70% (s), (D) Time to peak 70% (s), (E) Fractional shortening (%). Background symbols represent single cardiomyocytes. Darker-shade symbols represent male mice. Mean ± SEM. *$p < 0.05$ within one animal group, compared their own baseline (vehicle). $^{\#}p < 0.05$ compared to PTL within one animal group. $^{\dagger}p < 0.05$ compared to ISO within one animal group. (For interpretation of the references to colour in this figure legend, the reader is referred to the web version of this article.)

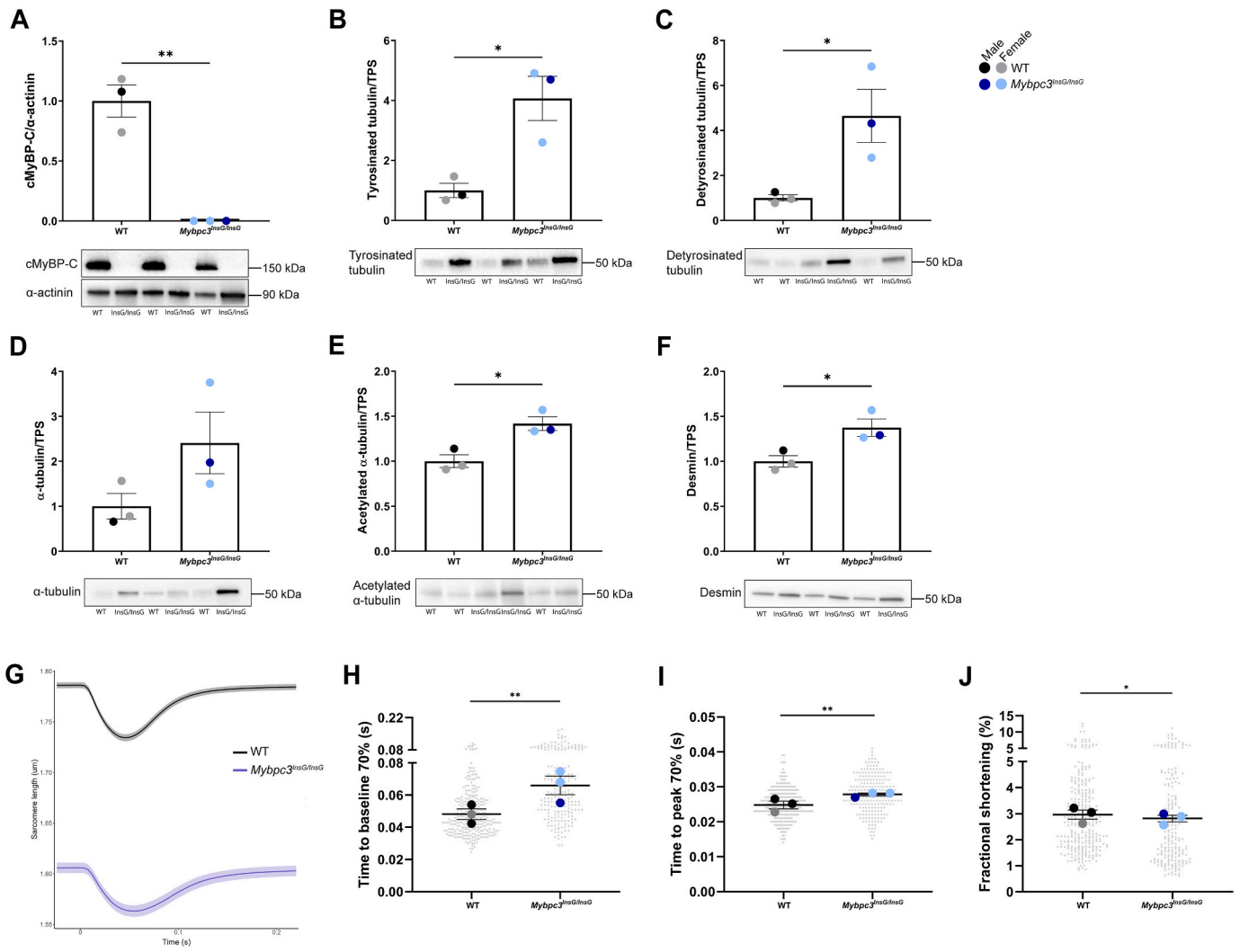

Fig. 6. HCM-associated changes in 3–4 week old *Mybpc3*$^{InsG/InsG}$ mice. (A) cMyBP-C protein levels relative to α-actinin in WT (n = 3, black/grey) and *Mybpc3*$^{InsG/InsG}$ mice (n = 3, blue). (B-F) Desmin, tyrosinated tubulin, detyrosinated tubulin, α-tubulin, and acetylated-α-tubulin levels of WT (n = 3) and *Mybpc3*$^{InsG/InsG}$ (n = 3) mice relative to total protein stain (Supplementary material). (G-J) Unloaded shortening measurements of 3–4 week old WT (N/n = 3/294, black/grey) and *Mybpc3*$^{InsG//InsG}$ (N/n = 3/208, blue) cardiomyocytes. (G) Averaged contraction-relaxation traces of cardiomyocytes, (H) Time to baseline 70% (s), (I) Time to peak 70% (s), (J) Fractional shortening (%). Background symbols represent single cardiomyocytes. Darker-shade symbols represent male mice. Mean ± SEM. *$p < 0.05$, **$p < 0.01$. (For interpretation of the references to colour in this figure legend, the reader is referred to the web version of this article.)

diastolic dysfunction. Heterozygous mice displayed a similar cardiac phenotype to WT mice. An HCM phenotype is likely to be present from an young age, as in 3–4 week old *Mybpc3*$^{InsG/InsG}$ mice, as cardiomyocyte contraction-relaxation kinetics were impaired, and the non-sarcomere cytoskeleton, akin to 18–28 week old *Mybpc3*$^{InsG/InsG}$ cardiomyocytes, shifted towards a stiffer profile due to increased desmin and tubulin detyrosination. Furthermore, unloaded shortening experiments revealed slowed contraction and relaxation kinetics of *Mybpc3*$^{InsG/InsG}$ cardiomyocytes. When treating 18–28 week old *Mybpc3*$^{InsG/InsG}$ cardiomyocytes with PTL, contraction duration shortened, and ISO treatment accelerated the rate of relaxation. Combining PTL + ISO further improved kinetics of relaxation of *Mybpc3*$^{InsG/InsG}$ cardiomyocytes.

Although LV fibrosis was somewhat increased in *Mybpc3*$^{InsG/InsG}$ mice, it was not significantly different from WT and *Mybpc3*$^{+/InsG}$ mice. This may be due to intra-animal model variability in the degree of fibrosis, which has been noted in the few other cMyBP-C mouse models, where fibrosis was increased in homozygous mice [29,30], but not in neonatal homozygous mice [31], nor in heterozygous mice [32]. Moreover, large variety in the degree of fibrosis is also found in HCM patient studies [26,33] and is often classified as a hallmark of late-stage HCM [33,34]. However, an earlier hallmark of HCM, cardiomyocyte hypertrophy, was present in the *Mybpc3*$^{InsG/InsG}$ model. At 3–4 weeks of age, a trend towards cardiac hypertrophy was observed as HW/BW doubled compared to a small sample of WT HW/BW measurements. This is similar to HW/BW ratios noted in other cMyBP-C null models [30,35]. Although HW was assessed, this is representative of ventricular hypertrophy as VW constitutes at least 60%, up to 80% of HW in mice [36,37]. At 18–28 weeks old, VW/BW of *Mybpc3*$^{InsG/InsG}$ was also significantly greater than WT and *Mybpc3*$^{+/InsG}$ mice. The enlarged CSA of 18–28 week old *Mybpc3*$^{InsG/InsG}$ mice is also is in line with findings from cardiac tissue of HCM mutation carriers, where CSA was increased compared to non-failing donors [38], as well as in another cMyBP-C null neonatal mouse model [31]. We did not detect changes to cardiomyocyte CSA in *Mybpc3*$^{+/InsG}$ mice, similar to another heterozygous cMyBP-C mouse model [32]. Of note, fractional shortening significantly decreased and $LVID_d$ was enlarged in our homozygous *Mybpc3*$_{c.2373InsG}$ model, displaying overall hypocontractility. The enlarged CSA and increased $LVID_d$ with decreased fractional shortening fit a late-stage (clinical class IV) HCM phenotype with systolic dysfunction [18]. Taken together, our

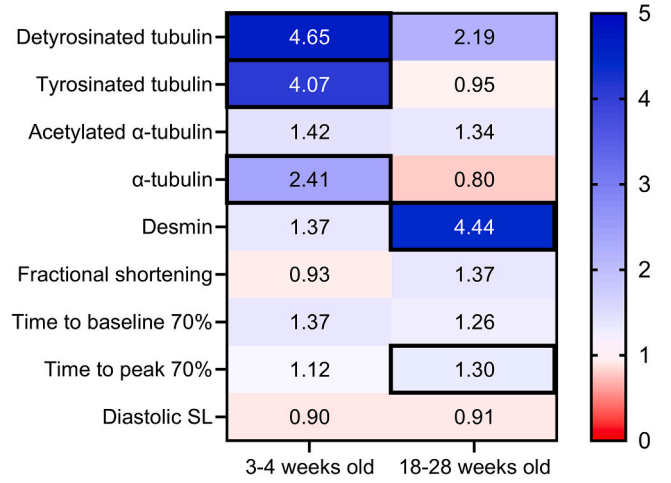

Fig. 7. Comparison of changes in 3–4 week old and 18–28 week old *Mybpc3*$^{InsG/InsG}$ mice. Normalized to age-matched WT. 1 (white) = no change compared to WT, red = fold decrease compared to WT, blue = fold increase compared to WT. Significant differences ($p < 0.05$) are indicated by the borders surrounding the cells. Independent samples *t*-test. (For interpretation of the references to colour in this figure legend, the reader is referred to the web version of this article.)

Mypbc3$_{c.2373InsG}$ homozygous mouse is a representative model of end-stage HCM, as in vivo and histological hallmarks of HCM are present at 18–28 weeks of age.

Thus far, the few studies of cMyBP-C null mouse models that have been described, report contrasting findings regarding cardiomyocyte Ca^{2+} sensitivity. Harris et al. [39] found Ca^{2+} sensitivity to be decreased in homozygous cMyBP-C mice, whereas Ca^{2+} handling was unaltered in other models [30,40–42]. On the other hand, Fraysse et al. [43] and Najafi et al. [44,45] reported increased Ca^{2+} sensitivity in heterozygous and homozygous *Mybpc3* point mutation mice. In HCM patients, increased Ca^{2+} sensitivity has been reported consistently, including in *MYBPC3* mutation carriers [5,46,47]. This is due to diminished stimulation of the β-adrenergic pathway in HCM [48], which reduces PKA-dependent phosphorylation of its targets, including cTnI [14]. In turn, cTnI hypophosphorylation, impairs relaxation as Ca^{2+} dissociation from the troponin complex is hampered [49]. Our unloaded shortening data indeed demonstrates slowed contraction-relaxation kinetics of cardiomyocytes from both 3–4 week old and 18–28 week old *Mybpc3*$^{InsG/InsG}$ mice. Moreover, bi-phosphorylated cTnI was significantly reduced in *Mybpc3*$^{InsG/InsG}$ mice. Impaired contractile kinetics may therefore be, in part, caused by altered cTnI phosphorylation profile in the homozygous *Mypbc3*$_{c.2373InsG}$ mice. Reduced bi-phosphorylated cTnI, with the majority of cTnI dephosphorylated, has also been detected in myectomy tissue of HCM patients compared to donors in a proteomic analysis [12], Phos-Tag analysis [50], and specifically in myectomy tissue of *MYBPC3* mutation carriers [5].

Pharmacologically targeting the blunted β-adrenergic pathway and PKA-dependent phosphorylation in *Mybpc3*$^{InsG/InsG}$ mice and HCM patients could rescue relaxation kinetics [13,14,51]. Here, we demonstrate that PKA-dependent phosphorylation, mediated by β-adrenergic receptor agonist ISO, indeed accelerated relaxation in homozygous *Mybpc3*$_{c.2373InsG}$ mouse cardiomyocytes. *Mybpc3*$^{+/InsG}$ cardiomyocytes were largely unaffected upon increased β-adrenergic activity, suggesting that there may be mild impairment of cardiomyocyte contraction-relaxation kinetics, although no phenotype of HCM was observed. Of note, the yield of living cell after cell isolation was considerably lower in *Mybpc3*$^{InsG/InsG}$ mice. Also, a higher number of *Mybpc3*$^{InsG/InsG}$ cardiomyocytes either did not survive ISO treatment or showed contraction artefacts that made them not suitable for downstream analysis. This accounts for the variation in number of cardiomyocytes measured per pharmacological treatment.

Another striking feature of *Mybpc3*$^{InsG/InsG}$ cardiomyocytes is their shorter diastolic SL. This is not uncommon to *Mybpc3*-mutated mouse models [43]. Pharmacologically, SL of homozygous *Mybpc3* mutated mice could be corrected with cross-bridge inhibitor 2,3-butanedione monoxime (BDM), indicating that these cells are already partly activated during diastole [43]. In our model, SL could only partially be corrected with BDM (Supplementary Fig. S5). Also, fractional shortening of homozygous *Mybpc3*$_{c.2373InsG}$ cardiomyocytes did not increase further with PTL or PTL + ISO treatment. Possibly, the shorter diastolic SL accounts for this. Yet, diastolic SL did not correlate to peak height (we plotted against peak height instead of fractional shortening as fractional shortening is dependent on diastolic SL, Supplementary Fig. S3D), in line with previous analyses of a large-scale rat cardiomyocyte contractility study [22].

Furthermore, altered cytoskeletal protein composition also contributes to impaired cardiomyocyte contraction-relaxation kinetics, and tubulin detyrosination is associated with increased cardiomyocyte stiffness [27,52]. We previously reported increased levels of detyrosinated tubulin levels in HCM patients and *Mybpc3*$^{InsG/InsG}$ mice [21] and, indeed, contraction and relaxation duration of 18–28 week old *Mybpc3*$^{InsG/InsG}$ cardiomyocytes were prolonged compared to WT and *Mybpc3*$^{+/InsG}$ mice, which was also noted in 3–4 week old *Mybpc3*$^{InsG/InsG}$ cardiomyocytes. Tubulin detyrosination is known to shift the cardiomyocyte cytoskeleton towards a stiffer profile [27,28]. Pharmacologically, tubulin detyrosination was suppressed in isolated 18–28 week old *Mybpc3*$^{InsG/InsG}$ cardiomyocytes by PTL, a tubulin carboxypeptidase inhibitor [52]. This ameliorated relaxation time of *Mybpc3*$^{InsG/InsG}$ cardiomyocytes, partially restoring contractile function in these cells, as cytoskeletal stiffness is rescued due to diminished levels of detyrosinated tubulin. This has also been observed in rat cardiomyocytes, where treatment with PTL increased relaxation duration in comparison to baseline measurements [53].

Detyrosinated tubulin interacts with desmin, coupling microtubules to sarcomeres [21,27]. As the connected microtubules need to deform when sarcomeres shorten, this affects contraction-relaxation kinetics of *Mybpc3*$^{InsG/InsG}$ cardiomyocytes due to the stiffer tubulin signature. Our homozygous *Mybpc3*$_{c.2373InsG}$ model had elevated desmin levels, further contributing to cardiomyocyte stiffness. This in line with research where knock-out of desmin resulted in a disorganized and more compliant microtubule network compared to WT cells [27]. PTL is only able to partially rescue contractile function of *Mybpc3*$^{InsG/InsG}$ cardiomyocytes. In this model, the absence of cMyBP-C also contributes to contractile dysfunction, since it is required for interaction with myosin heavy chain to aid cross-bridge kinetics [8,9]. Moreover, heterozygous *Mybpc3*$_{c.2373InsG}$ cardiomyocytes, which contain cMyBP-C, did not have impaired contraction-relaxation kinetics. Their response to PTL was also dampened, as their tubulin signature was unaltered. Impaired relaxation kinetics are therefore, in part, due to increased tubulin detyrosination, as is evident from the correcting effect of PTL. This is further supported by the fact that acetylated α-tubulin, another PTM associated with cardiomyocyte stiffness and slows contraction-relaxation kinetics [54], was similar amongst all groups.

Similar to the 18–28 week old *Mybpc3*$^{InsG/InsG}$ mice, detyrosinated tubulin and desmin were increased in 3–4 week old *Mybpc3*$^{InsG/InsG}$ mice, as well as having elevated acetylated α-tubulin levels and a (non-significant) trend towards increased α-tubulin. Overall, both healthy tubulin signature and that of a stiffer cytoskeletal profile were elevated in the 3–4 week old *Mybpc3*$_{c.2373InsG}$ model. Possibly, the compensatory mechanism of PTMs is progressing in the this and stabilizing towards a stiffer profile at an older age. This is similar to tubulin signatures of stage II HCM patients without obstruction and end-stage HCM patients with heart failure [55].

Our heterozygous *Mybpc3*$_{c.2373InsG}$ mice did not develop classical hallmarks of HCM at an early-adult stage. Two other cMyBP-C mutation models [35,37,56] have shown similar findings [30,40]. The

heterozygous models were generated to be haploinsufficient for cMyBP-C, while the model described in this study was generated to study the patient-specific *MYBPC3*$_{c.2373InsG}$ mutation and was not cMyBP-C haploinsufficient. However, the heterozygous models of McConnell et al. and Vignier et al. have been studied with secondary disease triggers such as ageing [57], transverse aortic constriction [58], and recently Western diet [59], resulting in the development of an HCM phenotype. This indicates that the effect of this mutation may be evident at an advanced age or in metabolically compromised mice.

To conclude, our adult homozygous mouse model of the most common Dutch founder mutation, *MYBPC3*$_{c.2373InsG}$, is representative of disease pathogenicity in mutation carrying patients with severe phenotypic expression of HCM. HCM is present with different pathogenic expression in the 3–4 week old homozygous *Mybpc3*$_{c.2373InsG}$ model. Assessing the effect of this mutation in advanced age or metabolically compromised heterozygous *Mybpc3*$_{c.2373InsG}$ models, and cardiac function and remodeling in young homozygous *Mybpc3*$_{c.2373InsG}$ mice, may yield additional insight into the development of HCM. The combination of the 3–4 week and 18–28 week old homozygous *Mybpc3*$_{c.2373InsG}$ models is nevertheless a robust choice to study potential therapeutic targets and pathophysiology of developing HCM.

Funding

This work was supported by the Netherlands Cardiovascular Research (CVON) and Dutch CardioVascular Alliance (DCVA) initiatives of the Dutch Heart Foundation (2020B005 DCVA-DOUBLE-DOSE), and NWO-ZonMW (91818602 VICI grant).

Author contributions

SH drafted the manuscript, designed and performed experiments, analyzed and interpreted data. MS designed and performed experiments, and analyzed data. MG, VJ, and SM performed experiments. LMD designed experiments. EM analyzed data. FGS edited manuscript. JV conceptualized research, edited and approved manuscript. DWDK conceptualized research, designed experiments, interpreted data, edited and approved manuscript.

Disclosures

None.

Data availability

Data will be shared upon reasonable request to the corresponding author.

Acknowledgements

We thank Teodora Georgieva and Thomas Doetschmann for creating the knock-in mouse model. We also thank Sakthivel Sadayappan for providing us with antibodies for cMyBP-C pS273, pS282, and pS302. Graphical abstract was created with BioRender.com.

Appendix A. Supplementary data

Supplementary data to this article can be found online at https://doi.org/10.1016/j.yjmcc.2023.10.008.

References

[1] C. Semsarian, J. Ingles, M.S. Maron, B.J. Maron, New perspectives on the prevalence of hypertrophic cardiomyopathy, J. Am. Coll. Cardiol. 65 (12) (2015) 1249–1254.
[2] J. van der Velden, G.J.M. Stienen, Cardiac disorders and pathophysiology of Sarcomeric proteins, Physiol. Rev. 99 (1) (2019) 381–426.
[3] B.A. Maron, R.S. Wang, M.R. Carnethon, E.J. Rowin, J. Loscalzo, B.J. Maron, et al., What causes hypertrophic cardiomyopathy? Am. J. Cardiol. 179 (2022) 74–82.
[4] M. Alders, R. Jongbloed, W. Deelen, A. van den Wijngaard, P. Doevendans, F. Ten Cate, et al., The 2373insG mutation in the MYBPC3 gene is a founder mutation, which accounts for nearly one-fourth of the HCM cases in the Netherlands, Eur. Heart J. 24 (20) (2003) 1848–1853.
[5] S.J. van Dijk, E.R. Paalberends, A. Najafi, M. Michels, S. Sadayappan, L. Carrier, et al., Contractile dysfunction irrespective of the mutant protein in human hypertrophic cardiomyopathy with normal systolic function, Circ. Heart Fail. 5 (1) (2012) 36–46.
[6] S. Marston, O. Copeland, A. Jacques, K. Livesey, V. Tsang, W.J. McKenna, et al., Evidence from human myectomy samples that MYBPC3 mutations cause hypertrophic cardiomyopathy through haploinsufficiency, Circ. Res. 105 (3) (2009) 219–222.
[7] A.M. Jacques, O. Copeland, A.E. Messer, C.E. Gallon, K. King, W.J. McKenna, et al., Myosin binding protein C phosphorylation in normal, hypertrophic and failing human heart muscle, J. Mol. Cell. Cardiol. 45 (2) (2008) 209–216.
[8] M. Gruen, H. Prinz, M. Gautel, cAPK-phosphorylation controls the interaction of the regulatory domain of cardiac myosin binding protein C with myosin-S2 in an on-off fashion, FEBS Lett. 453 (3) (1999) 254–259.
[9] M.J. Previs, S. Beck Previs, J. Gulick, J. Robbins, D.M. Warshaw, Molecular mechanics of cardiac myosin-binding protein C in native thick filaments, Science. 337 (6099) (2012) 1215–1218.
[10] C.W. Tong, J.E. Stelzer, M.L. Greaser, P.A. Powers, R.L. Moss, Acceleration of crossbridge kinetics by protein kinase a phosphorylation of cardiac myosin binding protein C modulates cardiac function, Circ. Res. 103 (9) (2008) 974–982.
[11] R.W. Kensler, R. Craig, R.L. Moss, Phosphorylation of cardiac myosin binding protein C releases myosin heads from the surface of cardiac thick filaments, Proc. Natl. Acad. Sci. U. S. A. 114 (8) (2017) E1355–E1364.
[12] J. Zhang, M.J. Guy, H.S. Norman, Y.C. Chen, Q. Xu, X. Dong, et al., Top-down quantitative proteomics identified phosphorylation of cardiac troponin I as a candidate biomarker for chronic heart failure, J. Proteome Res. 10 (9) (2011) 4054–4065.
[13] R. Zhang, J. Zhao, A. Mandveno, J.D. Potter, Cardiac troponin I phosphorylation increases the rate of cardiac muscle relaxation, Circ. Res. 76 (6) (1995) 1028–1035.
[14] J.C. Kentish, D.T. McCloskey, J. Layland, S. Palmer, J.M. Leiden, A.F. Martin, et al., Phosphorylation of troponin I by protein kinase a accelerates relaxation and crossbridge cycle kinetics in mouse ventricular muscle, Circ. Res. 88 (10) (2001) 1059–1065.
[15] C.Y. Ho, C. Carlsen, J.J. Thune, O. Havndrup, H. Bundgaard, F. Farrohi, et al., Echocardiographic strain imaging to assess early and late consequences of sarcomere mutations in hypertrophic cardiomyopathy, Circ. Cardiovasc. Genet. 2 (4) (2009) 314–321.
[16] T. Germans, I.K. Russel, M.J. Gotte, M.D. Spreeuwenberg, P.A. Doevendans, Y. M. Pinto, et al., How do hypertrophic cardiomyopathy mutations affect myocardial function in carriers with normal wall thickness? Assessment with cardiovascular magnetic resonance, J. Cardiovasc. Magn. Reson. 12 (1) (2010) 13.
[17] A.J. Marian, E. Braunwald, Hypertrophic cardiomyopathy: genetics, pathogenesis, clinical manifestations, diagnosis, and therapy, Circ. Res. 121 (7) (2017) 749–770.
[18] M. Michels, I. Olivotto, F.W. Asselbergs, J. van der Velden, Life-long tailoring of management for patients with hypertrophic cardiomyopathy: awareness and decision-making in changing scenarios, Neth. Hear. J. 25 (3) (2017) 186–199.
[19] M.W. Wessels, J.C. Herkert, I.M. Frohn-Mulder, M. Dalinghaus, A. van den Wijngaard, R.R. de Krijger, et al., Compound heterozygous or homozygous truncating MYBPC3 mutations cause lethal cardiomyopathy with features of noncompaction and septal defects, Eur. J. Hum. Genet. 23 (7) (2015) 922–928.
[20] J. van der Velden, F.W. Asselbergs, J. Bakkers, S. Batkai, L. Bertrand, C.R. Bezzina, et al., Animal models and animal-free innovations for cardiovascular research: current status and routes to be explored. Consensus document of the ESC working group on myocardial function and the ESC working group on cellular biology of the heart, Cardiovasc. Res. 118 (15) (2022) 3016–3051.
[21] M. Schuldt, J. Pei, M. Harakalova, L.M. Dorsch, S. Schlossarek, M. Mokry, et al., Proteomic and functional studies reveal Detyrosinated tubulin as treatment target in sarcomere mutation-induced hypertrophic cardiomyopathy, Circ. Heart Fail. 14 (1) (2021), e007022.
[22] E.E. Nollet, E.M. Manders, M. Goebel, V. Jansen, C. Brockmann, J. Osinga, et al., Large-scale contractility measurements reveal large atrioventricular and subtle interventricular differences in cultured unloaded rat cardiomyocytes, Front. Physiol. 11 (2020) 815.
[23] F. Ahmad, J.G. Seidman, C.E. Seidman, The genetic basis for cardiac remodeling, Annu. Rev. Genomics Hum. Genet. 6 (2005) 185–216.
[24] B.J. Maron, S. Mackey-Bojack, E. Facile, E. Duncanson, E.J. Rowin, M.S. Maron, Hypertrophic cardiomyopathy and sudden death initially identified at autopsy, Am. J. Cardiol. 127 (2020) 139–141.
[25] J. Shirani, R. Pick, W.C. Roberts, B.J. Maron, Morphology and significance of the left ventricular collagen network in young patients with hypertrophic cardiomyopathy and sudden cardiac death, J. Am. Coll. Cardiol. 35 (1) (2000) 36–44.
[26] B. Raman, R. Ariga, M. Spartera, S. Sivalokanathan, K. Chan, S. Dass, et al., Progression of myocardial fibrosis in hypertrophic cardiomyopathy: mechanisms and clinical implications, Eur. Heart J. Cardiovasc. Imaging 20 (2) (2019) 157–167.
[27] P. Robison, M.A. Caporizzo, H. Ahmadzadeh, A.I. Bogush, C.Y. Chen, K. B. Margulies, et al., Detyrosinated microtubules buckle and bear load in contracting cardiomyocytes, Science. 352 (6284) (2016) aaf0659.

[28] M.A. Caporizzo, C.Y. Chen, K. Bedi, K.B. Margulies, B.L. Prosser, Microtubules increase diastolic stiffness in failing human cardiomyocytes and myocardium, Circulation. 141 (11) (2020) 902–915.
[29] C.I. Berul, B.K. McConnell, H. Wakimoto, I.P. Moskowitz, C.T. Maguire, C. Semsarian, et al., Ventricular arrhythmia vulnerability in cardiomyopathic mice with homozygous mutant myosin-binding protein C gene, Circulation. 104 (22) (2001) 2734–2739.
[30] D. Barefield, M. Kumar, P.P. de Tombe, S. Sadayappan, Contractile dysfunction in a mouse model expressing a heterozygous MYBPC3 mutation associated with hypertrophic cardiomyopathy, Am. J. Physiol. Heart Circ. Physiol. 306 (6) (2014) H807–H815.
[31] E.T. Farrell, A.C. Grimes, W.J. de Lange, A.E. Armstrong, J.C. Ralphe, Increased postnatal cardiac hyperplasia precedes cardiomyocyte hypertrophy in a model of hypertrophic cardiomyopathy, Front. Physiol. 8 (2017) 414.
[32] Y. Cheng, X. Wan, T.A. McElfresh, X. Chen, K.S. Gresham, D.S. Rosenbaum, et al., Impaired contractile function due to decreased cardiac myosin binding protein C content in the sarcomere, Am. J. Physiol. Heart Circ. Physiol. 305 (1) (2013) H52–H65.
[33] I. Olivotto, F. Cecchi, C. Poggesi, M.H. Yacoub, Patterns of disease progression in hypertrophic cardiomyopathy: an individualized approach to clinical staging, Circ. Heart Fail. 5 (4) (2012) 535–546.
[34] M. Habib, A. Adler, K. Fardfini, S. Hoss, K. Hanneman, E.J. Rowin, et al., Progression of myocardial fibrosis in hypertrophic cardiomyopathy: a cardiac magnetic resonance study, JACC Cardiovasc. Imaging 14 (5) (2021) 947–958.
[35] N. Vignier, S. Schlossarek, B. Fraysse, G. Mearini, E. Krämer, H. Pointu, et al., Nonsense-mediated mRNA decay and ubiquitin–proteasome system regulate cardiac myosin-binding protein C mutant levels in cardiomyopathic mice, Circ. Res. 105 (3) (2009) 239–248.
[36] K.P. Roos, M.C. Jordan, M.C. Fishbein, M.R. Ritter, M. Friedlander, H.C. Chang, et al., Hypertrophy and heart failure in mice overexpressing the cardiac sodium-calcium exchanger, J. Card. Fail. 13 (4) (2007) 318–329.
[37] R. Amin, I. Muthuramu, J.P. Aboumsallem, M. Mishra, F. Jacobs, B. De Geest, Selective HDL-raising human Apo A-I gene therapy counteracts cardiac hypertrophy, reduces myocardial fibrosis, and improves cardiac function in mice with chronic pressure overload, Int. J. Mol. Sci. 18 (9) (2017) 2012.
[38] E.R. Witjas-Paalberends, C. Ferrara, B. Scellini, N. Piroddi, J. Montag, C. Tesi, et al., Faster cross-bridge detachment and increased tension cost in human hypertrophic cardiomyopathy with the R403Q MYH7 mutation, J. Physiol. 592 (15) (2014) 3257–3272..
[39] S.P. Harris, C.R. Bartley, T.A. Hacker, K.S. McDonald, P.S. Douglas, M.L. Greaser, et al., Hypertrophic cardiomyopathy in cardiac myosin binding protein-C knockout mice, Circ. Res. 90 (5) (2002) 594–601..
[40] B.K. McConnell, K.A. Jones, D. Fatkin, L.H. Arroyo, R.T. Lee, O. Aristizabal, et al., Dilated cardiomyopathy in homozygous myosin-binding protein-C mutant mice, J. Clin. Invest. 104 (9) (1999) 1235–1244.
[41] S. Merkulov, X. Chen, M.P. Chandler, J.E. Stelzer, In vivo cardiac myosin binding protein C gene transfer rescues myofilament contractile dysfunction in cardiac myosin binding protein C null mice, Circ. Heart Fail. 5 (5) (2012) 635–644.
[42] J. Li, R. Mamidi, C.Y. Doh, J.B. Holmes, N. Bharambe, R. Ramachandran, et al., AAV9 gene transfer of cMyBPC N-terminal domains ameliorates cardiomyopathy in cMyBPC-deficient mice, JCI Insight. 5 (17) (2020), e130182..
[43] B. Fraysse, F. Weinberger, S.C. Bardswell, F. Cuello, N. Vignier, B. Geertz, et al., Increased myofilament Ca2+ sensitivity and diastolic dysfunction as early consequences of Mybpc3 mutation in heterozygous knock-in mice, J. Mol. Cell. Cardiol. 52 (6) (2012) 1299–1307.
[44] A. Najafi, S. Schlossarek, E.D. van Deel, N. van den Heuvel, A. Guclu, M. Goebel, et al., Sexual dimorphic response to exercise in hypertrophic cardiomyopathy-associated MYBPC3-targeted knock-in mice, Pflugers Arch. 467 (6) (2015) 1303–1317..
[45] A. Najafi, V. Sequeira, M. Helmes, I.A. Bollen, M. Goebel, J.A. Regan, et al., Selective phosphorylation of PKA targets after beta-adrenergic receptor stimulation impairs myofilament function in Mybpc3-targeted HCM mouse model, Cardiovasc. Res. 110 (2) (2016) 200–214.
[46] V. Sequeira, P.J. Wijnker, L.L. Nijenkamp, D.W. Kuster, A. Najafi, E.R. Witjas-Paalberends, et al., Perturbed length-dependent activation in human hypertrophic cardiomyopathy with missense sarcomeric gene mutations, Circ. Res. 112 (11) (2013) 1491–1505.
[47] T. Tucholski, W. Cai, Z.R. Gregorich, E.F. Bayne, S.D. Mitchell, S.J. McIlwain, et al., Distinct hypertrophic cardiomyopathy genotypes result in convergent sarcomeric proteoform profiles revealed by top-down proteomics, Proc. Natl. Acad. Sci. U. S. A. 117 (40) (2020) 24691–24700.
[48] A. Najafi, V. Sequeira, D.W. Kuster, J. van der Velden, Beta-adrenergic receptor signalling and its functional consequences in the diseased heart, Eur. J. Clin. Investig. 46 (4) (2016) 362–374.
[49] V. Kooij, M. Saes, K. Jaquet, R. Zaremba, D.B. Foster, A.M. Murphy, et al., Effect of troponin I Ser23/24 phosphorylation on Ca2+−sensitivity in human myocardium depends on the phosphorylation background, J. Mol. Cell. Cardiol. 48 (5) (2010) 954–963.
[50] A.E. Messer, C.E. Gallon, S.B. Marston, Analysis of cardiac myofibrillar troponin I phosphorylation in normal and failing human hearts using Phos-tags, Biophys. J. 96 (3) (2009).
[51] V. Rao, Y. Cheng, S. Lindert, D. Wang, L. Oxenford, A.D. McCulloch, et al., PKA phosphorylation of cardiac troponin I modulates activation and relaxation kinetics of ventricular myofibrils, Biophys. J. 107 (5) (2014) 1196–1204.
[52] X. Fonrose, F. Ausseil, E. Soleilhac, V. Masson, B. David, I. Pouny, et al., Parthenolide inhibits tubulin carboxypeptidase activity, Cancer Res. 67 (7) (2007) 3371–3378.
[53] M.A. Caporizzo, C.Y. Chen, A.K. Salomon, K.B. Margulies, B.L. Prosser, Microtubules provide a viscoelastic resistance to myocyte motion, Biophys. J. 115 (9) (2018) 1796–1807.
[54] A.K. Coleman, H.C. Joca, G. Shi, W.J. Lederer, C.W. Ward, Tubulin acetylation increases cytoskeletal stiffness to regulate mechanotransduction in striated muscle, J. Gen. Physiol. 153 (7) (2021), e202012743.
[55] S. Algül, L. Dorsch, O. Sorop, A. Vink, M. Michels, C.G. dos Remedios, et al., The microtubule signature in cardiac disease: Etiology, disease stage and age dependency, J. Comp. Physiol. B. 193 (5) (2023) 581–595.
[56] S. Sadayappan, J. Gulick, H. Osinska, L.A. Martin, H.S. Hahn, G.W. Dorn 2nd, et al., Cardiac myosin-binding protein-C phosphorylation and cardiac function, Circ. Res. 97 (11) (2005) 1156–1163.
[57] B. McConnell, D. Fatkin, C. Semsarian, K. Jones, D. Georgakopoulous, C. Maguire, et al., Comparison of two murine models of familial hypertrophic cardiomyopathy, Circ. Res. 88 (2001) 383–389.
[58] D. Barefield, M. Kumar, J. Gorham, J.G. Seidman, P.P. de Tombe, S. Sadayappan, Haploinsufficiency of MYBPC3 exacerbates the development of hypertrophic cardiomyopathy in heterozygous mice, JMCC. 79 (2015) 234–243.
[59] E.E. Nollet, S. Algül, M. Goebel, S. Schlossarek, N.N. van der Wel, J.J.M. Jans, et al., Western diet triggers cardiac dysfunction in heterozygous Mybpc3-targeted knock-in mice: a two-hit model of hypertrophic cardiomyopathy, JMCC PLUS. 6 (2023), 100050.